Downloaded from jnm.snmjournals.org by on March 15, 2017. For personal use only.

^{18}F-FET PET Differentiation of Ring-Enhancing Brain Lesions

Frank W. Floeth[1], Dirk Pauleit[2], Michael Sabel[1], Guido Reifenberger[3], Gabriele Stoffels[2], Walter Stummer[1], Frank Rommel[1], Kurt Hamacher[4], and Karl-Josef Langen[2]

[1]Department of Neurosurgery, Heinrich-Heine-University, Düsseldorf, Germany; [2]Institute of Medicine and Brain Imaging Center West, Research Center Jülich, Jülich, Germany; [3]Department of Neuropathology, Heinrich-Heine-University, Düsseldorf, Germany; and [4]Institute of Nuclear Chemistry and Brain Imaging Center West, Research Center Jülich, Jülich, Germany

The aim of this study was to explore the differential diagnostic value of PET using the amino acid *O*-(2-^{18}F-fluoroethyl)-L-tyrosine (^{18}F-FET) in patients with newly diagnosed solitary intracerebral lesions showing ring enhancement on contrast-enhanced MRI. **Methods:** ^{18}F-FET PET analyses were performed on 14 consecutive patients with intracerebral ring-enhancing lesions. Eleven of the patients were additionally studied with ^{18}F-FDG PET. In all patients, the main differential diagnosis after MRI was a malignant lesion, in particular glioblastoma multiforme, versus a benign lesion, in particular brain abscess. A malignant tumor was suspected for lesions showing increased ^{18}F-FET uptake on PET images with a mean lesion-to-brain ratio of at least 1.6 (^{18}F-FET PET positive). A nonneoplastic lesion was suspected in cases of minimal or absent ^{18}F-FET uptake, with a mean lesion-to-brain ratio of less than 1.6 (^{18}F-FET PET negative). Histologic diagnosis was obtained by serial biopsies in 13 of the 14 patients. One patient refused the biopsy, but follow-up indicated an abscess because his lesion regressed under antibiotic therapy. **Results:** Histology and clinical follow-up showed high-grade malignant gliomas in 5 patients and nonneoplastic lesions in 9 patients. The findings of ^{18}F-FET PET were positive in all 5 glioma patients and in 3 of 9 patients with nonneoplastic lesions, including 2 patients with brain abscesses and 1 patient with a demyelinating lesion. The findings of ^{18}F-FDG PET were positive (mean lesion-to-gray matter ratio $\geq$ 0.7) in 4 of 4 glioma patients and 3 of 7 patients with nonneoplastic lesions. **Conclusion:** Although ^{18}F-FET PET has been shown to be valuable for the diagnostic evaluation of brain tumors, our data indicate that, like ^{18}F-FDG PET, ^{18}F-FET PET has limited specificity in distinguishing between neoplastic and nonneoplastic ring-enhancing intracerebral lesions. Thus, histologic investigation of biopsy specimens remains mandatory to make this important differential diagnosis.

Key Words: ring enhancement; ^{18}F-FET PET; abscess; glioblastoma

J Nucl Med 2006; 47:776–782

The differential diagnosis of solitary intracerebral ring-enhancing lesions on contrast-enhanced MRI includes different types of malignant tumors, as well as various benign, nonneoplastic lesions. Among the tumors, high-grade glioma, in particular glioblastoma multiforme, and metastasis, most commonly metastatic carcinomas of the lung or breast, are the main differential diagnoses. Nonneoplastic masses that may appear as ring-enhancing lesions include intracerebral abscesses (including toxoplasmosis and fungal abscesses), demyelinating and reactive/resorptive lesions (acute inflammatory demyelination, resolving hematoma or infarction, radiation necrosis) and parasitic lesions (cysticercosis cyst, pork tapeworm). Because of the known uncertainties about the accuracy of MRI for noninvasive assessment of brain lesions (*1,2*), several attempts have been made to improve brain tumor diagnostics by metabolic imaging using PET and SPECT. Radiolabeled amino acids proved to be useful tracers for brain tumor diagnostics (*3,4*). Encouraging data showing improved tumor delineation with PET have been reported, especially with PET using [methyl-^{11}C]-L-methionine (^{11}C-MET) (*5–13*). Because of the short physical half-life of the ^{11}C label (20 min), however, ^{11}C-MET remains restricted to a few PET centers with a cyclotron on site and cannot become established in routine clinical practice.

The recently developed ^{18}F-labeled amino acid *O*-(2-^{18}F-fluoroethyl)-L-tyrosine (^{18}F-FET) can be synthesized with high radiochemical yields, thus allowing large-scale production for clinical purposes (*14,15*). Initial clinical studies using ^{18}F-FET PET in human brain tumors have shown results similar to those for ^{11}C-MET PET (*16,17*). ^{18}F-FET PET has been reported to allow tumor recurrence to be distinguished from radiation-induced changes in cases of suspected recurrent high- and low-grade gliomas (*18*). In addition, we have shown that delineation of the cellular tumor mass of human gliomas is better by ^{18}F-FET PET than by MRI alone (*19,20*). In a prospective study of 50 patients with newly diagnosed lesions, we found that ^{18}F-FET PET had a high specificity for the detection of both high- and low-grade gliomas and could serve as a useful

Received Dec. 16, 2005; revision accepted Jan. 24, 2006.
For correspondence or reprints contact: Karl-Josef Langen, Institute of Medicine, Research Center Jülich, P.O. Box 1913, D-52425 Jülich, Germany.
E-mail: k.j.langen@fz-juelich.de

Downloaded from jnm.snmjournals.org by on March 15, 2017. For personal use only.

tool for the diagnostic assessment of suspected glioma lesions, in particular concerning biopsy site planning (*21*).

For ^{11}C-MET PET, several cases of significant tracer accumulation in histologically confirmed brain abscesses have been reported (*22–25*). Recent data from animal experiments indicate that ^{18}F-FET, in contrast to ^{11}C-MET and ^{18}F-FDG, exhibits low uptake in nonneoplastic inflammatory cells and in inflammatory lymph nodes, thus promising a higher specificity for the detection of tumors (*26,27*).

The aim of the present prospective study was to explore the potential of ^{18}F-FET PET for distinguishing between neoplastic and nonneoplastic solitary ring-enhancing lesions in humans.

MATERIALS AND METHODS

Patient Population

From June 2001 to June 2005, we screened 373 patients with newly diagnosed intracerebral mass lesions for the following inclusion criteria: an isolated solitary intracranial lesion with ring-shaped enhancement and central hypointensity on gadolinium-enhanced MRI but without solid or nodular enhancing areas; no systemic signs of infection, such as fever, nuchal rigidity, leukocytosis, or elevated C-reactive protein; and stable clinical and neurologic status without signs of increased intracranial pressure, thus allowing for elective management. The exclusion criteria included pretreated or multiple lesions; ring-enhancing lesions with areas of nodular enhancement; progressive clinical or neurologic deterioration with signs of increased intracranial pressure, thus necessitating emergency management; and clinical signs of infection, such as fever, nuchal rigidity, leukocytosis, or elevated C-reactive protein, indicating an active brain abscess requiring urgent puncture.

Within the 5-y study period, a total of 18 patients presented with a newly diagnosed solitary ring-enhancing lesion. Four of these patients had to be excluded: Two patients had large lesions with a midline shift and rapid clinical deterioration requiring emergency decompression. Glioblastoma multiforme was diagnosed in both patients. Two patients had signs of acute meningeal infection, such as fever, nuchal rigidity, or an elevated level of C-reactive protein, and in one of these patients the symptoms occurred in combination with a severely reduced neurologic status requiring emergency puncture. Purulent brain abscesses were found in both patients.

Finally, a total of 14 patients with solitary ring-enhancing lesions were able to undergo elective management including preoperative metabolic imaging with ^{18}F-FET PET. Eleven patients (patients 1, 3–6, and 8–13) were additionally investigated by preoperative PET with ^{18}F-FDG. Histologic diagnoses were obtained through neuronavigated biopsies in 13 patients. One patient (patient 2) refused the biopsy, and empiric antibiotic therapy was administered for 4 mo without a histologic diagnosis. The further course of this patient confirmed the working diagnosis of an intracerebral abscess; that is, MRI follow-up demonstrated continuous regression of his brain lesion, and MRI 1 y after diagnosis showed complete resolution of the lesion.

Initial symptoms were seizures in 8 patients and focal neurologic deficits in 6 patients. Eight patients presented with space-occupying lesions causing a mass effect (ventricular compression, midline shift), whereas the remaining 6 patients showed lesions without a significant mass effect. All patients had supratentorial lesions, 13 of which were lobar and 1 deep seated. Nine lesions were right hemispheric and 5 were left hemispheric. Detailed data on the individual patients is provided in Table 1. The study was

TABLE 1
Clinical Data

Patient no.	Age (y)	Sex	Histologic diagnosis	Location	Size*	ROI†	Seizure‡	Mass effect¶	Edema§	Bacteria‖
1	67	M	Abscess	R, T	+	7.2	+	+	+	−
2	53	M	Abscess	R, T	−	4.4	+	−	−	−
3	62	M	Abscess	L, P	+	5.2	+	−	−	+
4	51	M	Abscess	R, P	+	6.7	+	+	+	−
5	44	M	Abscess	R, ganglia	−	5.9	−	+	+	+
6	24	M	Empyema	L, frontal	+	6.5	−	−	−	+
7	50	F	Demyelination	L, frontal	+	1.9	+	+	+	
8	62	M	Hemorrhage	R, frontal	+	8.2	−	+	+	
9	57	M	Hemorrhage	R, T	+	4.1	−	+	+	
10	64	M	GBM	R, frontal	+	4.3	−	+	+	
11	45	M	AA	R, T-P	+	7.8	+	−	−	
12	53	M	GBM	R, T	+	2.4	+	−	−	
13	62	M	GBM	L, frontal	+	4.1	+	−	−	
14	69	M	GBM	L, O	+	8.1	−	+	+	

*Plus sign indicates that maximal diameter of ring-enhancing lesion was >3 cm.
†Values are size of ROI (cm^2) placed on contrast-enhancing ring on MR image.
‡Plus sign indicates that patient presented with seizures as initial symptom.
¶Plus sign indicates that lesion was space occupying, with ventricular compression and midline shift.
§Plus sign indicates that extent of perifocal edema was >2 cm.
‖Plus sign indicates that bacteria were found in pus cultures.
R = right hemispheric; T = temporal; L = left hemispheric; P = parietal; GBM = glioblastoma multiforme WHO grade IV; AA = anaplastic astrocytoma WHO grade III; O = occipital.

Downloaded from jnm.snmjournals.org by on March 15, 2017. For personal use only.

approved by the local institutional review board at the Medical Faculty of Heinrich-Heine-University Düsseldorf and by federal authorities. All subjects gave written informed consent to participate in the study.

MRI

MRI examinations were performed on a 1.5-T system (Sonata; Siemens). The conventional imaging protocol consisted of a T1-weighted 3-dimensional magnetization-prepared rapid-acquisition gradient-echo sequence (field of view, 25 cm; matrix, 205 × 256; repetition time, 2,200 ms; echo time, 3.9 ms; inversion time, 1,200 ms; flip angle, 15; number of slices, 128; slice thickness, 1.5 mm; slice gap, 0 mm; number of signals averaged, 1; time of acquisition, 6:38 min) before and 2 min after injection of 20 mL of gadolinium-diethylenetriaminepentaacetic acid (Magnevist; Schering) and a transversal fluid-attenuation inversion-recovery sequence (field of view, 25 cm; matrix, 205 × 256; repetition time, 9,000 ms; echo time, 119 ms; inversion time, 2,500 ms; flip angle, 90; number of slices, 25; slice thickness, 5 mm; slice gap, 0 mm; number of signals averaged, 2; time of acquisition, 4:32 min).

^{18}F-FET PET

The amino acid ^{18}F-FET was produced via phase transfer–mediated nucleophilic ^{18}F-fluorination of *N*-trityl-*O*-(2-tosyloxyethyl)-L-tyrosine tert-butyl ester and subsequent deprotection (*14*). The uncorrected radiochemical yield was about 35% at a specific radioactivity of greater than 200 GBq/μmol and a radiochemical purity of greater than 98%. PET studies were acquired 15–40 min after intravenous injection of 200 MBq of ^{18}F-FET, which was administered as an isotonic neutral solution. The measurements were performed on an ECAT EXACT HR+ scanner (Siemens Medical Systems) in 3-dimensional mode (32 rings, 15.5-cm axial field of view). For attenuation correction, transmission scans with 3 ^{68}Ge/^{68}Ga rotating line sources were measured. After correction for random and scattered coincidences and dead time, image data were obtained by filtered backprojection in Fourier space using the ECAT 7.2 software (direct inverse Fourier transformation; Shepp filter, 2.48 mm in full width at half maximum; pixel size, 2 × 2 × 2.4 mm). The reconstructed images were decay corrected; the reconstructed image resolution was about 5.5 mm.

Preoperative MRI and ^{18}F-FET PET were coregistered using dedicated software (MPI tool, version 3.28; ATV). Because most of the benign lesions exhibited indifferent ^{18}F-FET uptake, an objective positioning of regions of interest (ROIs) on the PET scans based on threshold values was impossible. Therefore, irregular ROIs were placed manually on the contrast-enhancing ring on MR images and transferred to the coregistered ^{18}F-FET and ^{18}F-FDG PET scans. Information on the size of the ROIs is given in Table 1. A larger reference ROI was placed on contralateral normal-appearing brain, including white and gray matter. Mean and maximal standardized uptake values of ^{18}F-FET were calculated by dividing the radioactivity (kBq/mL) of the ROIs by the radioactivity injected per gram of body weight for the corresponding PET scans. Mean and maximal lesion-to-brain ratios were calculated by dividing the mean and maximal ROI value of the lesion by the mean ROI value of the normal brain in the ^{18}F-FET PET scan (^{18}F-FET ratio). In a previous biopsy-controlled study, we found for tissue samples corresponding to normal and peritumoral tissue a mean lesion-to-brain ratio of 1.2 ± 0.4 (n = 26) for ^{18}F-FET uptake (*20*). Therefore, a mean lesion-to-brain ratio of 1.6 was taken as the threshold for distinguishing between malignant and benign lesions. A lesion with a tracer uptake ratio of less than 1.6 was judged as ^{18}F-FET negative, and a lesion with a ratio of at least 1.6 was judged as ^{18}F-FET positive.

^{18}F-FDG PET

^{18}F-FDG was synthesized as previously described (*28*). The average specific radioactivity was greater than 200 GBq/μmol. The PET studies with ^{18}F-FDG were done on a different day within 1 wk before or after the ^{18}F-FET study. PET scans were acquired 30–60 min after intravenous injection of 200 MBq of ^{18}F-FDG, which was administered as an isotonic neutral solution. The methods of reconstruction and attenuation correction were the same as described for ^{18}F-FET. The ^{18}F-FDG scans were coregistered to the preoperative MR images and to the ^{18}F-FET PET scans as already described. The ROIs for the ring-enhancing lesions as used in the ^{18}F-FET scans were transferred to the corresponding ^{18}F-FDG scans. Because ^{18}F-FDG uptake in gray matter is different from ^{18}F-FDG uptake in white matter, the reference ROI for normal brain was different from that in the ^{18}F-FET scans. A circular ROI was placed on contralateral gray matter, and mean and maximal lesion-to-brain ratios were calculated by dividing the mean and maximal ROI values of the lesion by the mean value of the cortical ROI in the ^{18}F-FDG PET scan (^{18}F-FDG ratio). A mean lesion-to-brain ratio of 0.7 was taken as the threshold for distinguishing between malignant and benign lesions (*29*). A lesion with a tracer uptake ratio of less than 0.7 was judged as ^{18}F-FDG negative, and a lesion with a ratio of at least 0.7 was judged as ^{18}F-FDG positive.

Neuronavigated Biopsy Procedure

MRI data were incorporated into the neuronavigation system. For coregistration, anatomic landmarks and external cutaneous fiducial markers were used in each examination. Tissue samples were collected in all cases from both the outer area of ring enhancement and the inner area of hypointensity. The biopsies were sampled with the aid of a standard stereotactic biopsy cannula, which was referenced to the neuronavigation system and connected to an adjustable Leyla arm. Through a small skin incision and a standard 8-mm burr hole, the cannula was placed under neuronavigated control into the area of interest. A 2-mm stereotactic forceps was used to obtain at least 5 and at most 12 biopsy specimens.

Histopathology

Routine histologic sections of each biopsy specimen were assessed by an experienced neuropathologist after they had been fixed in formalin and embedded in paraffin. Neoplastic lesions were classified according to the World Health Organization (WHO) classification of tumors of the nervous system (*30*). If necessary, immunohistochemical analyses were performed on formalin-fixed paraffin sections according to standard protocols, including staining for glial fibrillary acidic protein, neurofilament protein, myelin basic protein, macrophage/microglia marker CD68, lymphocytic markers (CD3, CD20, CD45), and the proliferation marker Ki-67 (MIB1). A conclusive histologic diagnosis was made for all 13 biopsied patients.

RESULTS

Histologic investigation revealed malignant gliomas in 5 of 14 patients, with 4 lesions corresponding histologically

Downloaded from jnm.snmjournals.org by on March 15, 2017. For personal use only.

to glioblastomas of WHO grade IV and 1 lesion to anaplastic astrocytoma of WHO grade III. All 4 glioblastomas and the 1 anaplastic astrocytoma were ^{18}F-FET positive. ^{18}F-FDG PET was performed on 4 glioma patients (3 glioblastomas and 1 anaplastic astrocytoma) and had positive findings in all cases. Data on standardized uptake values and mean and maximal lesion-to-brain ratios are given in Table 2.

In 9 patients, benign nonneoplastic lesions were diagnosed, including 5 cases of brain abscess, 1 case of acute demyelinating disease, 1 subdural empyema, and 2 intracerebral hematomas in resorption. ^{18}F-FET PET had negative findings in 6 of 9 patients with benign lesions but (false) positive findings in 2 patients with brain abscess (Fig. 1) and in the patient with acute demyelination (Fig. 2). ^{18}F-FDG PET was performed on 7 patients and had negative findings in 4 patients but (false) positive findings in 2 patients with brain abscess and in 1 patient with subdural empyema.

Accumulation of ^{18}F-FET and ^{18}F-FDG in the investigated ring-enhancing lesions was always within the boundaries of the gadolinium enhancement on MR images (irrespective of histology). In some cases, the distribution of the tracer uptake was identical to the area of gadolinium enhancement, and in some cases, the area of tracer uptake was smaller than the area of gadolinium enhancement. No ^{18}F-FET or ^{18}F-FDG uptake occurred outside the area of gadolinium enhancement, that is, within the central hypointensity or the perifocal edema. Tracer uptake did not correlate with patient age, sex, lesion location, seizure activity, lesion size and mass effect, extent of perifocal edema, or detection of a causative organism in an abscess.

DISCUSSION

Because of the known uncertainties in the differential diagnosis of an intracerebral ring-enhancing lesion on CT and MRI (*31*), preoperative metabolic imaging with PET is under investigation as a novel tool for the noninvasive identification of benign or malignant ring-enhancing lesions. Numerous case reports and studies on small patient groups have demonstrated that the gold standards of PET—imaging with the glucose analog ^{18}F-FDG and the amino-acid ^{11}C-MET—cannot reliably predict whether a lesion is malignant. Several studies have shown accumulation of these tracers in brain abscesses (*23,24,32,33*). A more recent study on 4 patients with brain abscesses reported that pre- and postoperative PET scans demonstrated significant tracer accumulation of both ^{11}C-MET and ^{18}F-FDG in all lesions both before treatment and during antibiotic treatment after puncture of the abscesses (*25*). The area of increased ^{11}C-MET and ^{18}F-FDG uptake corresponded closely to the enhancing area on CT and MR images. The authors speculated that the mechanism of ^{11}C-MET uptake in the inflammatory area might be related to the higher metabolic rate and the active transport of amino acids, as well as to disruption of the blood–brain barrier. The mechanism of ^{18}F-FDG uptake was thought to be related to a higher metabolic rate and the increased density of inflammatory cells. It was concluded that PET images reflect the degree of inflammatory response in brain abscesses—thus suggesting that PET is useful in detecting inflammatory lesions and in assessing the clinical effects of antibiotic treatment (*25*).

In most cases of brain abscesses, the area of increased ^{11}C-MET and ^{18}F-FDG uptake corresponds closely to the

TABLE 2
PET Results

Patient no.	Histologic diagnosis	^{18}F-FET					^{18}F-FDG		
		SUVmax	SUVmean	SUVmax/BG	SUVmean/BG	Rating	SUVmax/cortex	SUVmean/cortex	Rating
1	Abscess	2.5	1.7	2.0	1.3	−	0.8	0.6	−
2	Abscess	2.7	1.9	1.8	1.3	−	—	—	NA
3	Abscess	2.7	2.2	2.6	2.1	+	1.5	0.9	+
4	Abscess	1.8	1.1	2.5	1.6	+	1.3	0.7	+
5	Abscess	1.3	1.0	1.5	1.2	−	0.9	0.5	−
6	Empyema	2.1	1.8	1.4	1.2	−	1.3	0.9	+
7	Demyelination	3.1	2.4	2.6	2.0	+	—	—	NA
8	Hemorrhage	1.7	1.2	1.9	1.3	−	1.1	0.6	−
9	Hemorrhage	2.1	1.8	1.7	1.4	−	1.0	0.7	−
10	GBM	4.5	3.0	4.0	2.7	+	2.3	1.6	+
11	AA	2.8	2.1	3.2	2.4	+	1.0	0.8	+
12	GBM	4.0	3.2	3.1	2.4	+	1.4	1.1	+
13	GBM	3.7	2.8	3.8	2.9	+	1.0	0.7	+
14	GBM	3.7	2.5	3.4	2.3	+	—	—	NA

SUVmax = maximum standardized uptake value; SUVmean = mean standardized uptake value; BG = background; plus sign indicates SUVmean/BG ≥ 1.6 (^{18}F-FET rating) or SUVmean/cortex ≥ 0.7 (^{18}F-FDG rating); NA = not applicable; GBM = glioblastoma multiforme WHO grade IV; AA = anaplastic astrocytoma WHO grade III.

Downloaded from jnm.snmjournals.org by on March 15, 2017. For personal use only.

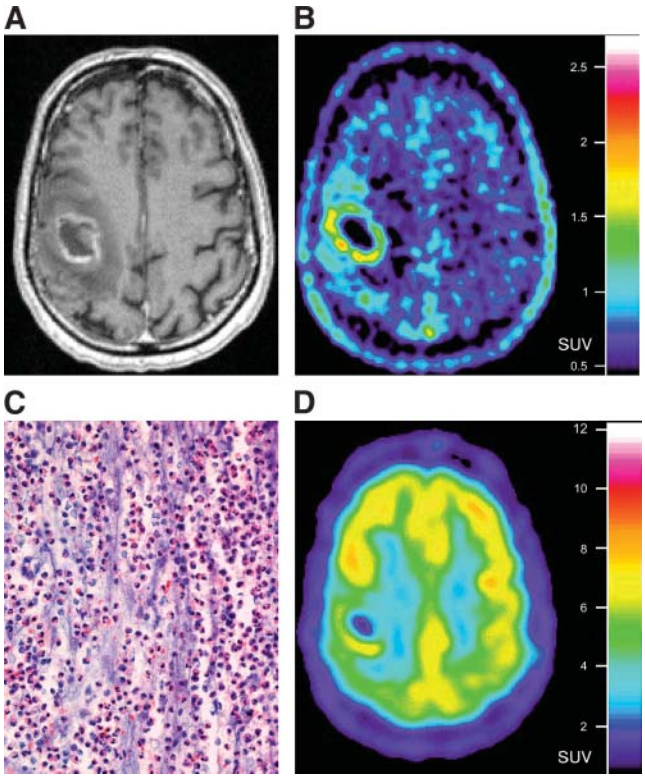


FIGURE 1. Intracerebral abscess in patient 4. (A) Gadolinium-enhanced MR image shows single right parietal ring-enhancing lesion. (B and D) ^{18}F-FET PET image (B) and ^{18}F-FDG PET image (D) demonstrate significant tracer uptake highly suggestive of malignant neoplastic lesion. (C) Photomicrograph of hematoxylin- and eosin-stained biopsy specimen reveals brain abscess with purulent content and partially necrotic granulocytes in fibrinoid exudations.

area of gadolinium enhancement on CT and MR images. However, on record are individual patients showing ^{18}F-FDG uptake within a brain abscess and not in the contrast-enhancing walls (*34*) or high uptake of both ^{11}C-MET and ^{18}F-FDG around a brain abscess (*22*). Taken together, these findings allow one to conclude that there is a frequent lesional accumulation of ^{11}C-MET and ^{18}F-FDG in patients with a brain abscess and that the uptake usually correlates with the disruption of the blood–brain barrier visible as gadolinium enhancement on MR images.

The amino acid ^{18}F-FET shows a high diagnostic accuracy in brain tumors (*21,22*), and experimental studies have indicated that ^{18}F-FET is more specific than ^{18}F-FDG and ^{11}C-MET in distinguishing inflammatory lesions from malignant lesions (*26,27*). Recently, a PET study of peripheral tumors demonstrated that ^{18}F-FET, unlike other tyrosine derivatives such as L-^{11}C-tyrosine, 2-^{18}F-fluoro-L-tyrosine, or L-3-^{18}F-fluoro-α-methyltyrosine, showed no uptake in lymphomas or in most adenocarcinomas (*35*). On the contrary, all squamous cell carcinomas turned out to be ^{18}F-FET positive in this study. Another report, on patients with squamous cell carcinomas of the neck, revealed low ^{18}F-FET uptake in inflammatory tissue surrounding the tumors, which themselves exhibited high ^{18}F-FDG uptake (*36*). The investigators speculated that a selective transport of ^{18}F-FET via subtype 2 of the amino acid transport system L might account for the rather selective accumulation of ^{18}F-FET in certain tumor types and the low uptake in inflammatory tissue (*35*).

The result of the present pilot study on ring-enhancing brain lesions indicates that the situation in the brain may be different from that in peripheral tissue. We observed a significant uptake of ^{18}F-FET in 2 of 5 brain abscesses. It remains to be elucidated which specific cellular components other than macrophages in brain lesions lead to the increased ^{18}F-FET uptake. In any case, high ^{18}F-FET uptake in a ring-enhancing lesion should be interpreted with caution and a biopsy remains necessary.

A diagnostic challenge in the field of ring-enhancing lesions is the distinction of acute inflammatory demyelination. Demyelinating disease may manifest in the form of a solitary lesion but often presents as multiple intracerebral ring- or ringlike-enhancing lesions. The main differential diagnoses include metastatic carcinoma, high-grade glioma, and brain abscess. In a retrospective analysis of 6 patients with histologically proven acute demyelination treated between 1990 and 2001, PET was performed in 2 cases to assess the metabolic activity of the lesions (*37*). The histopathologic diagnosis was established by stereotactic biopsy in 5 patients and by microsurgical resection of the lesion in 1 patient. In 1 patient, both ^{11}C-MET PET and ^{18}F-FDG PET were performed, and there was no uptake of either tracer. In another patient, only ^{11}C-MET PET was

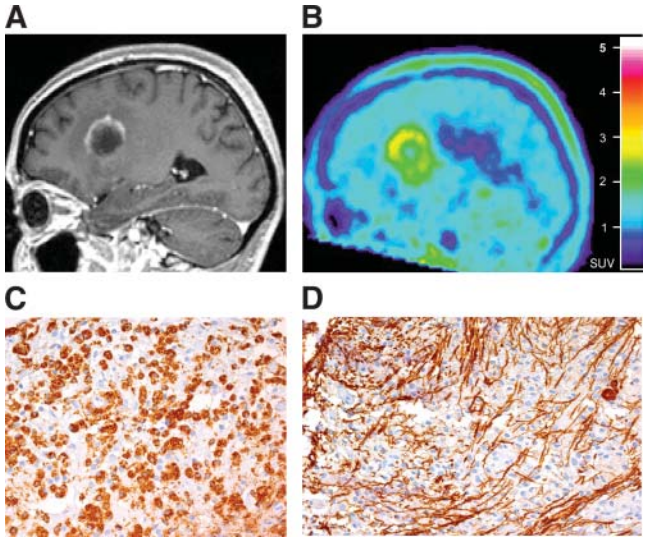


FIGURE 2. Demyelinating lesion in patient 7. (A) Gadolinium-enhanced MR image shows single left frontal ring-enhancing lesion. (B) ^{18}F-FET PET image reveals significant uptake indicative of neoplastic lesion. (C) Photomicrograph of biopsy specimen reveals acute demyelinating lesion with massive invasion of macrophages as indicated by immunostaining for CD68. (D) Immunohistochemistry for neurofilaments shows persisting axonal processes but also axonal damage within lesion.

Downloaded from jnm.snmjournals.org by on March 15, 2017. For personal use only.

performed, and the lesion showed only an unspecific, low uptake of the tracer (lesion-to-brain ratio, 1.25). In contrast to these observations, we detected marked ^{18}F-FET uptake (mean lesion-to-brain ratio, 2.0) in patient 7, who had an acute demyelinating lesion. This result indicated tumor, and additional investigation of this patient with single-voxel MRI spectroscopy supported the hypothesis of a neoplastic lesion: The spectra patterns were typical, showing a high concentration of choline (indicating cellular proliferation) and the absence of *N*-acetyl-aspartate (denoting loss of neurons), with an *N*-acetyl-aspartate–to–choline ratio of 0.5. However, histologic examination revealed an acute inflammatory demyelinating lesion with massive invasion of macrophages. With steroid medication, the lesion nearly disappeared within 3 mo, but all tests for multiple sclerosis were negative at that time. Six months later, typical periventricular lesions developed and the diagnosis of multiple sclerosis was established.

A limitation of our study might be that static ^{18}F-FET scans were acquired only from 15 to 40 min after injection. ^{18}F-FET uptake usually reaches a maximum approximately 15 min after injection, and tumor-to-brain ratios have shown only a minor decrease up to 60 min after injection (*17*). During the first 15 min after injection, the tracer concentration in the blood pool is high and may mimic pathologic ^{18}F-FET uptake in benign lesions—for example, in aneurysms (*38*). Therefore, imaging during the first 15 min after injection was avoided in our study.

A recent study found that a dynamic acquisition of ^{18}F-FET uptake might be helpful in differentiating between high-grade and low-grade gliomas (*38*). Although low-grade gliomas exhibited increasing tumor-to-brain ratios at 0–10 min after injection, compared with at 30–40 min after injection, decreasing tumor-to-brain ratios were observed for high-grade gliomas. However, because gliomas may exhibit both increasing and decreasing tumor-to-brain ratios, it is unlikely that a dynamic evaluation will be helpful in differentiating gliomas, abscesses, and demyelinating processes.

Taken together, our data indicate that metabolic imaging using ^{18}F-FET PET does not appear to be sufficiently specific to allow for a reliable noninvasive distinction between neoplastic and nonneoplastic intracerebral ring-enhancing lesions. Therefore, a histologic diagnosis should be attempted in all such patients. Although a morbidity ranging from 1% to 2% and lethal outcome in rare cases has to be tolerated (*39*), stereotactic or neuronavigated biopsy remains the method of choice to obtain the firm diagnosis that is necessary to guide adequate treatment.

CONCLUSION

Although ^{18}F-FET PET has been demonstrated to be a useful method to detect the extent of gliomas and to differentiate tumor recurrences from unspecific posttherapeutic changes in brain tissue, our data indicate that in newly diagnosed solitary intracerebral ring-enhancing lesions, ^{18}F-FET PET is not able to distinguish reliably between benign nonneoplastic lesions and malignant gliomas. High uptake may occur in cases of brain abscess and in acute inflammatory demyelination. In accordance with previous findings, ^{18}F-FDG PET did not improve the predictive value of preoperative imaging. Therefore, a biopsy with sampling of tissue specimens for neuropathologic evaluation remains the gold standard to establish a definite diagnosis in patients with newly diagnosed intracerebral ring-enhancing lesions.

ACKNOWLEDGMENTS

The authors thank Suzanne Schaden, Elisabeth Theelen, Barbara Elghahwagi, and Gabriele Oefler for assistance with the patient studies and Silke Grafmüller, Bettina Palm, and Erika Wabbals for radiosynthesis of ^{18}F-FET. This work was supported by the Brain Imaging Center West and a grant from the Deutsche Krebshilfe (70-3088-Sa I). The facility for MRI at the Institute of Medicine–Research Center Juelich was supported by the Bundesministerium für Bildung und Forschung grant BMBF 01GO0104.

REFERENCES

1. Pirzkall A, Nelson SJ, McKnight TR, et al. Metabolic imaging of low-grade gliomas with three-dimensional magnetic resonance spectroscopy. *Int J Radiat Oncol Biol Phys.* 2002;53:1254–1264.
2. Vigneron D, Bollen A, McDermott M, et al. Three-dimensional magnetic resonance spectroscopic imaging of histologically confirmed brain tumors. *Magn Reson Imaging.* 2001;19:89–101.
3. Jager PL, Vaalburg W, Pruim J, et al. Radiolabeled amino acids: basic aspects and clinical applications in oncology. *J Nucl Med.* 2001;42:432–445.
4. Langen KJ. Amino acid transport studies in brain tumors. In: Feinendegen LE, Shreeve WW, Eckelman WC, Bahk YW, Wagner HN Jr, eds. *Molecular Nuclear Medicine: The Challenge of Genomics and Proteomics to Clinical Practice.* Heidelberg, Germany: Springer-Verlag Berlin; 2003:477–485.
5. Braun V, Dempf S, Weller R, et al. Cranial neuronavigation with direct integration of (11)C methionine positron emission tomography (PET) data: results of a pilot study in 32 surgical cases. *Acta Neurochir (Wien).* 2002;144:777–782.
6. Chung JK, Kim YK, Kim SK, et al. Usefulness of ^{11}C-methionine PET in the evaluation of brain lesions that are hypo- or isometabolic on ^{18}F-FDG PET. *Eur J Nucl Med Mol Imaging.* 2002;29:176–182.
7. Derlon JM, Chapon F, Noel MH, et al. Non-invasive grading of oligodendrogliomas: correlation between in vivo metabolic pattern and histopathology. *Eur J Nucl Med.* 2000;27:778–787.
8. Derlon JM, Petit-Taboue MC, Chapon F, et al. The in vivo metabolic pattern of low-grade brain gliomas: a positron emission tomographic study using ^{18}F-fluorodeoxyglucose and ^{11}C-L-methylmethionine. *Neurosurgery.* 1997;40:276–287.
9. De Witte O, Goldberg I, Wikler D, et al. Positron emission tomography with injection of methionine as a prognostic factor in glioma. *J Neurosurg.* 2001;95:746–750.
10. Herholz K, Holzer T, Bauer B, et al. ^{11}C-Methionine PET for differential diagnosis of low-grade gliomas. *Neurology.* 1998;50:1316–1322.
11. Langen KJ, Ziemons K, Kiwit JC, et al. 3-[^{123}I]iodo-alpha-methyltyrosine and [methyl-^{11}C]-L-methionine uptake in cerebral gliomas: a comparative study using SPECT and PET. *J Nucl Med.* 1997;38:517–522.
12. Nuutinen J, Sonninen P, Lehikoinen P, et al. Radiotherapy treatment planning and long-term follow-up with [(11)C]methionine PET in patients with low-grade astrocytomas. *Int J Radiat Oncol Biol Phys.* 2000;48:43–52.
13. Sato N, Suzuki M, Kuwata N, et al. Evaluation of the malignancy of glioma using ^{11}C-methionine positron emission tomography and proliferating cell nuclear antigen staining. *Neurosurg Rev.* 1999;22:210–214.

Downloaded from jnm.snmjournals.org by on March 15, 2017. For personal use only.

14. Wester HJ, Herz M, Weber W, et al. Synthesis and radiopharmacology of O-(2-[^{18}F]fluoroethyl)-L-tyrosine for tumor imaging. *J Nucl Med.* 1999;40: 205–212.
15. Hamacher K, Coenen HH. Efficient routine production of the ^{18}F-labelled amino acid O-2-[^{18}F] fluoroethyl-L-tyrosine. *Appl Radiat Isot.* 2002;57: 853–856.
16. Langen KJ, Jarosch M, Muhlensiepen H, et al. Comparison of fluorotyrosines and methionine uptake in F98 rat gliomas. *Nucl Med Biol.* 2003;30: 501–508.
17. Weber WA, Wester HJ, Grosu AL, et al. O-(2-[^{18}F]fluoroethyl)-L-tyrosine and L-[methyl-^{11}C]methionine uptake in brain tumours: initial results of a comparative study. *Eur J Nucl Med.* 2000;27:542–549.
18. Pöpperl G, Gotz C, Rachinger W, et al. Value of O-(2-[(18)F]fluoroethyl)-L-tyrosine PET for the diagnosis of recurrent glioma. *Eur J Nucl Med Mol Imaging.* 2004;31:1464–1470.
19. Messing-Juenger AM, Floeth FW, Pauleit D, et al. Multimodal target point assessment for stereotactic biopsy in children with diffuse bithalamic astrocytomas. *Childs Nerv Syst.* 2002;18:445–449.
20. Pauleit D, Floeth F, Hamacher K, et al. O-(2-[^{18}F]fluoroethyl)-L-tyrosine PET combined with MRI improves the diagnostic assessment of cerebral gliomas. *Brain.* 2005;128:678–687.
21. Floeth FW, Pauleit D, Wittsack HJ, et al. Multimodal metabolic imaging of cerebral gliomas: positron emission tomography with [^{18}F]fluoroethyl-L-tyrosine and magnetic resonance spectroscopy. *J Neurosurg.* 2005;102:318–327.
22. Dethy S, Manto M, Kentos A, et al. PET findings in a brain abscess associated with a silent atrial septal defect. *Clin Neurol Neurosurg.* 1995;97:349–353.
23. Ishii K, Ogawa T, Hatazawa J, et al. High L-methyl-[^{11}C]methionine uptake in brain abscess: a PET study. *J Comput Assist Tomogr.* 1993;17:660–661.
24. Mineura K, Sasajima T, Kowada M, et al. Indications for differential diagnosis of nontumor central nervous system diseases from tumors: a positron emission tomography study. *J Neuroimaging.* 1997;7:8–15.
25. Tsuyuguchi N, Sunada I, Ohata K, et al. Evaluation of treatment effects in brain abscess with positron emission tomography: comparison of fluorine-18-fluorodeoxyglucose and carbon-11-methionine. *Ann Nucl Med.* 2003;17: 47–51.
26. Kaim AH, Weber B, Kurrer MO, et al. ^{18}F-FDG and ^{18}F-FET uptake in experimental soft tissue infection. *Eur J Nucl Med Mol Imaging.* 2002;29: 648–654.
27. Rau FC, Weber WA, Wester HJ, et al. O-(2-[^{18}F]fluoroethyl)-L-tyrosine (FET): a tracer for differentiation of tumour from inflammation in murine lymph nodes. *Eur J Nucl Med Mol Imaging.* 2002;29:1039–1046.
28. Hamacher K, Coenen HH, Stöcklin G. Efficient stereospecific synthesis of no-carrier-added 2-[^{18}F]-fluoro-2-deoxy-D-glucose using aminopolyether supported nucleophilic substitution. *J Nucl Med.* 1986;27:235–238.
29. Meyer PT, Schreckenberger M, Spetzger U, et al. Comparison of visual and ROI-based brain tumour grading using ^{18}F-FDG PET: ROC analyses. *Eur J Nucl Med.* 2001;28:165–174.
30. Kleihues P, Cavenee WK. *World Health Organization Classification of Tumours: Pathology and Genetics—Tumours of the Nervous System.* New York, NY: Oxford University Press; 2000.
31. Grimstad IA, Hirschberg H, Rootwelt K. ^{99m}Tc-Hexamethylpropyleneamine oxime leukocyte scintigraphy and C-reactive protein levels in the differential diagnosis of brain abscesses. *J Neurosurg.* 1992;77:732–736.
32. Kracht LW, Friese M, Herholz K, et al. Methyl-[(11)C]-L-methionine uptake as measured by positron emission tomography correlates to microvessel density in patients with glioma. *Eur J Nucl Med Mol Imaging.* 2003;30:868–873.
33. Sasaki M, Ichiya Y, Kuwabara Y, et al. Ringlike uptake of [^{18}F]FDG in brain abscess: a PET study. *J Comput Assist Tomogr.* 1990;14:486–487.
34. Meyer MA, Frey KA, Schwaiger M. Discordance between F-18 fluorodeoxyglucose uptake and contrast enhancement in a brain abscess. *Clin Nucl Med.* 1993;18:682–684.
35. Pauleit D, Stoffels G, Schaden W, et al. PET with O-(2-[^{18}F]fluoroethyl)-L-tyrosine (FET) in peripheral tumors: first clinical results. *J Nucl Med.* 2005;46:411–416.
36. Pauleit D, Zimmermann A, Stoffels G, et al. ^{18}F-FET PET compared with ^{18}F-FDG PET and CT in patients with head and neck cancer. *J Nucl Med.* 2006;47: 256–261.
37. Maarouf M, Kuchta J, Miletic H, et al. Acute demyelination: diagnostic difficulties and the need for brain biopsy. *Acta Neurochir (Wien).* 2003;145: 961–969.
38. Weckesser M, Langen KJ, Rickert CH, et al. O-(2-[^{18}F]fluoroethyl)-L-tyrosine PET in the clinical evaluation of primary brain tumors. *Eur J Nucl Med Mol Imaging.* 2005;32:422–429.
39. Kreth FW, Muacevic A, Medele R, et al. The risk of haemorrhage after image guided stereotactic biopsy of intra-axial brain tumors: a prospective study. *Acta Neurochir (Wien).* 2001;143:539–545.

Downloaded from jnm.snmjournals.org by on March 15, 2017. For personal use only.

JNM The Journal of NUCLEAR MEDICINE

^{18}F-FET PET Differentiation of Ring-Enhancing Brain Lesions

Frank W. Floeth, Dirk Pauleit, Michael Sabel, Guido Reifenberger, Gabriele Stoffels, Walter Stummer, Frank Rommel, Kurt Hamacher and Karl-Josef Langen

J Nucl Med. 2006;47:776-782.

This article and updated information are available at:
http://jnm.snmjournals.org/content/47/5/776

Information about reproducing figures, tables, or other portions of this article can be found online at:
http://jnm.snmjournals.org/site/misc/permission.xhtml

Information about subscriptions to JNM can be found at:
http://jnm.snmjournals.org/site/subscriptions/online.xhtml

The Journal of Nuclear Medicine is published monthly.
SNMMI | Society of Nuclear Medicine and Molecular Imaging
1850 Samuel Morse Drive, Reston, VA 20190.
(Print ISSN: 0161-5505, Online ISSN: 2159-662X)

© Copyright 2006 SNMMI; all rights reserved.

SNMMI SOCIETY OF NUCLEAR MEDICINE AND MOLECULAR IMAGING